Design of Switchable and Reconfigurable Semi-lumped Wideband Bandpass Filter

Yang Xiong, LiTian Wang, Wei Zhang, DouDou Pang, Fan Zhang, and Ming He

A switchable single-wideband (SWB)-to-dual-wideband (DWB) bandpass filter (BPF), which is realized by using lumped switches, is presented in this paper. By alternating the operation modes—ON and OFF—in which the ON mode is achieved by placing the capacitors at the switching spots and the OFF mode is achieved by replacing the capacitors with inductors, DWB-to-SWB BPF can be achieved on the same device. In addition, by changing the capacitor values, the center frequency (CF) of the lower passband of DWB BPF can be easily tuned from 1.69 GHz to 2.22 GHz, while the higher passband stays almost unchanged. As an example, an SWB-to-DWB BPF is designed, fabricated, and measured. This BPF exhibits good performance including wideband, high isolation, compact size, and ability to switch.

Keywords: Bandpass filter, Dual-wideband, Switchable wideband filter.

I. Introduction

The rapid development of wireless communication technology requires radio frequency (RF) front-end to be miniature, multifunctional, wideband, and multiband in recent decades. Therefore, microwave bandpass filters (BPFs) with high performance have been widely investigated using various techniques, which include the multi-mode resonator (MMR) [1]–[7], defected ground structure (DGS) [8]–[13], signal multi-path propagation [14]–[17], and combining several BPFs using common ports [18]–[20]. Owing to its simple structure, flexible regulation, and compact size, MMR is a very promising candidate in filter design. In [4], dual-/tri-band and ultra-wideband BPFs are implemented by using the same configuration of a single MMR by carefully arranging the resonant modes. However, poor out-of-band rejection should be improved. In order to overcome the drawback of poor out-of-band rejection, DGS has been widely used to improve the stopband. Various unit cells of DGS are listed in [8], including the U-shaped resonator, open-loop shaped resonator, and cross-shaped resonator. DGS provides an extra degree of freedom in design, in which the excitation and propagation of an electromagnetic wave can be manipulated by changing the dimensions and shape of a defected structure in the ground plane at the cost of increasing the complexity of fabrication. In [15], [16], tri-/quint-band BPFs are implemented using a signal multi-path propagation method, which can produce multiple transmission zeros between the adjacent passbands. In [18]–[20], the center frequencies (CFs) and the bandwidths can be easily controlled, but this suffers from the drawback of relatively larger circuit dimensions.

In order to meet the requirement of modern communication systems, it is imperative to develop BPFs with reconfigurable and switchable passbands. Recently,

Manuscript received Mar. 29, 2017; revised June 11, 2017; accepted July 3, 2017. This work was supported in part by the National Natural Science Foundation of China under Grants (61101018, 51002081, and 61171028), and in part by the Tianjin Research Program of Application Foundation and Advanced Technology (15JCQNJC01300).

Yang Xiong (xiongyang0291@163.com), LiTian Wang (564816068@qq.com), Wei Zhang (467253303@qq.com), DouDou Pang (1902172934@qq.com), and Fan Zhang (1196762435@qq.com) are with the College of Electronic Information and Optical Engineering, Nankai University, Tianjin, China.

Ming He (corresponding author, heming@nankai.edu.cn) is with the College of Electronic Information and Optical Engineering, Nankai University, Tianjin, China, and Tianjin Key Laboratory of Optoelectronic Sensor and Sensing Network Technology, Nankai University, Tianjin, China.

active switching or tuning elements such as the varactor diode [21]–[23], p-i-n diode [24]–[26], ferroelectric varactor [27], [28], and microelectromechanical system (MEMS) devices [29], [30] are widely used for reconfigurable and switchable BPF design.

In addition, using passive switching element [23], [27], [31] is also believed to be practical in reconfigurable BPF design. Although the filters [21]–[30] have fully demonstrated the performance of switching or reconfiguration, the high insertion loss in the passband, which is very common when active switching or tuning elements are used, should be further reduced. Moreover, BPFs with narrow bandwidth is insufficient to meet the requirements of high data rate, high transmission capacity, and multi-wideband services in modern communication systems.

Therefore, SWB/DWB BPFs should be developed to meet that requirement. In recent years, some SWB/DWB BPFs have been presented, among which the methods of MMR [1]–[3], [21], DGS [10]–[13], signal multi-path propagation [14], [17], and combing individual MMRs or BPFs [18], [19] are successfully applied to designing SWB/DWB BPFs. However, there are few reports on a switchable SWB-to-DWB BPF using passive switching elements.

In this paper, a switchable SWB-to-DWB BPF, which is realized by using lumped switches, is presented. The operating modes, ON and OFF, are determined by whether the switch is a capacitor or inductor. In this work, ON mode is realized by placing the capacitors at the switching spots, which corresponds to the DWB BPF, whereas OFF mode is realized by replacing the capacitors with inductors at the switch spots, which corresponds to an SWB BPF. In addition, by changing the lumped switches, reconfigurability is obtained for the same device. For validation, an SWB-to-DWB BPF is designed, fabricated, and measured, which shows that the experimental results are in good agreement with the full-wave electromagnetic simulation results.

II. Filter Design and Analysis

1. Prototype Structure

The transmission line model (TLM) of the initial structure is illustrated in Fig. 1, which consists of a multi-mode step impedance resonator (SIR) with shorted circuit. Owing to its symmetrical property, the classical even- and odd-mode analysis method is employed to analyze this structure. The equivalent even- and odd-mode circuits are shown in Figs. 1(b) and 1(c). According to the transverse

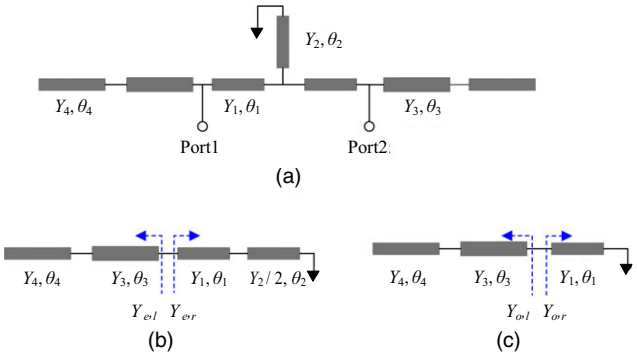

Fig. 1. Proposed (a) SIR, (b) even-mode equivalent circuit, and (c) odd-mode equivalent circuit.

resonant condition, we have

$$\mathrm{Im}(Y_{e,l} + Y_{e,r}) = 0, \tag{1}$$

$$\mathrm{Im}(Y_{o,l} + Y_{o,r}) = 0, \tag{2}$$

where

$$Y_{e,l} = \frac{jY_3(Y_4 \tan\theta_4 + Y_3 \tan\theta_3)}{Y_3 - Y_4 \tan\theta_4 \tan\theta_3}, \tag{3}$$

$$Y_{e,r} = \frac{jY_1(Y_1 \tan\theta_1 - Y_2 \cot\theta_2/2)}{Y_1 + Y_2 \cot\theta_2 \tan\theta_1/2}, \tag{4}$$

$$Y_{o,l} = \frac{jY_3(Y_4 \tan\theta_4 + Y_3 \tan\theta_3)}{Y_3 - Y_4 \tan\theta_4 \tan\theta_3}, \tag{5}$$

$$Y_{o,r} = -jY_1 \cot\theta_1. \tag{6}$$

Here, $Y_n (n = 1, 2, 3, 4)$ and $\theta_n (n = 1, 2, 3, 4)$ represent the corresponding stubs' characteristic admittances and electrical lengths, respectively. According to resonant conditions (1) and (2), we can derive the following equations:

$$\begin{aligned}&(k_3k_4 \tan\theta_4 + k_3^2 \tan\theta_3)(1 + 0.5 \cot\theta_2 \tan\theta_1) + \\ &(\tan\theta_1 - 0.5 \cot\theta_2)(k_3 - k_4 \tan\theta_4 \tan\theta_3) = 0,\end{aligned} \tag{7}$$

$$k_3 \cot\theta_1 - k_4 \tan\theta_4 \tan\theta_3 \cot\theta_1 - k_3k_4 \tan\theta_4 - k_3^2 \tan\theta_3 = 0, \tag{8}$$

where $k_3 = Y_3/Y_1$ and $k_4 = Y_4/Y_1$.

In order to understand the characteristics of the resonant frequencies of this structure fully, (3) and (4) have been solved to determine its real roots using the method of numerical calculation under variations of θ_2, θ_4, k_3, and k_4. As sketched in Fig. 2, six modes f_i (i = 1, 2, . . . , 6) are excited, among which f_1 and f_2 compose the 1st passband, and f_3, f_4, f_5, and f_6 form the 2nd passband. In this case, the other parameters will be fixed at $\theta_1 = 80°$, $\theta_2 = 20°$, $\theta_3 = 39°$, $\theta_4 = 59°$, $k_3 = 1.25$, and $k_4 = 0.8$ when a certain one is changed. As shown in Fig. 2(a), f_1, f_3, and f_5 shift down with an increase in θ_2, while the other resonant

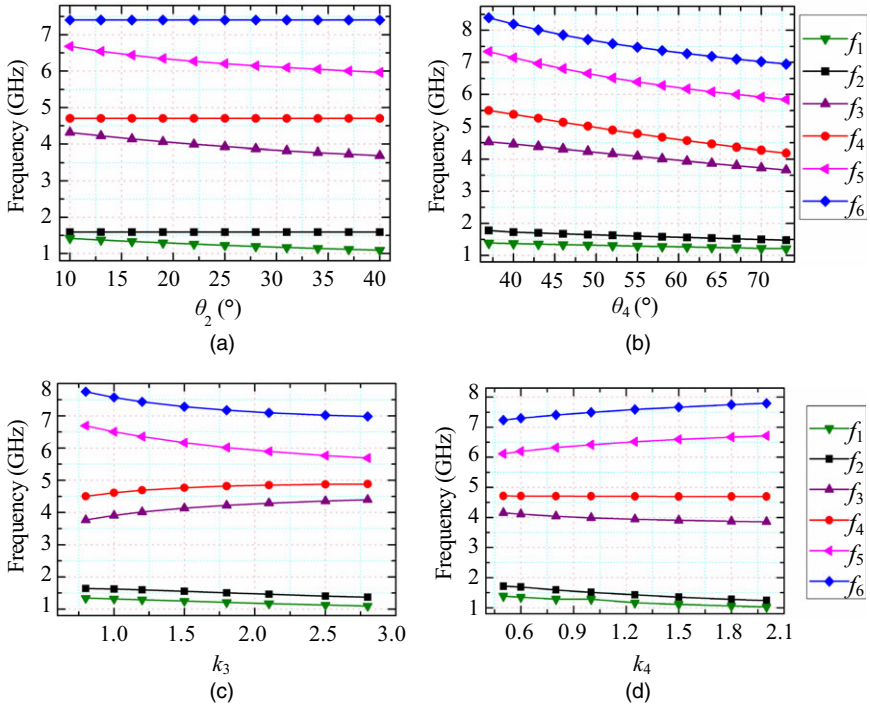

Fig. 2. Resonant frequencies versus (a) θ_2, (b) θ_4, (c) k_3, and (d) k_4.

frequencies are unchanged. It can be observed from Fig. 2(b) that the CF of the 2nd passband will shift down with an unchanged bandwidth, while the 1st passband has almost no influence. As depicted in Fig. 2 (c) and 2(d), k_3 and k_4 mainly affect the 2nd passband bandwidth with fixed CF, while it has the opposite trend as k_3 and k_4 become large.

2. SWB-to-DWB BPF

The configuration of the switchable SWB-to-DWB BPF is depicted in Fig. 3. Two switch elements are embedded in the stubs, whose physical lengths are equal to $L_1(L_{1L} + S_2 + L_{1R})$. As shown in Fig. 4(a), $|S_{21}|$ is simulated using TLM, where the switches are considered as two capacitors with a value of 1.1 pF. It can be found that six resonant modes are excited under the weak coupling, among which the first two modes are used to form the first passband, and the other four modes are

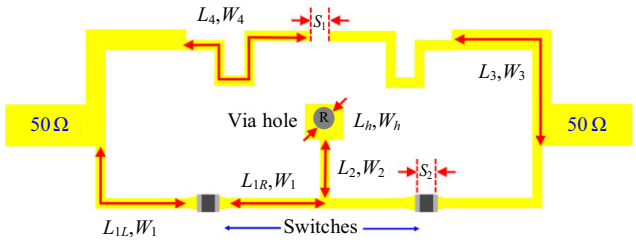

Fig. 3. Configuration of switchable SWB-to-DWB BPF.

employed to build the second one. In this design, source and load coupling determined by S_1 is employed, which is shown in Fig. 4(b).

The frequency responses of $|S_{21}|$ with a varied capacitor and W_3 are plotted in Fig. 5. It can be observed from Fig. 5(a) that capacitors mainly affect the 1st passband, but they have almost no influence on the 2nd passband. However, the situation is quite different when W_3 increases from 0.2 mm to 1 mm. W_3 mainly impacts the 2nd passband, whereas it has almost no effect on the 1st passband. As shown in Fig. 6, the CFs and fractional bandwidths (FBWs) are extracted using a full-wave electromagnetic simulator. It can be seen that CF and FBW of the 1st passband are mainly impacted by the capacitors, whereas the FBW of the 2nd passband is influenced by W_3. Therefore, the FBW of two passbands can be independently controlled by properly turning the capacitor and W_3.

When the switches operate in OFF mode, in which capacitors are replaced by inductors at the switch spots, the DWB BPF will switch to a SWB BPF, as shown in Fig. 7(a). The frequency responses of $|S_{21}|$ under the ON mode and OFF mode are simulated using a full-wave electromagnetic simulator. It can be observed that a DWB BPF is built when capacitors are employed, and an SWB BPF is formed when inductors are adopted. To understand the effects of the inductor on the SWB BPF, the frequency responses of the SWB BPF are simulated using a full-

https://doi.org/10.4218/etrij.17.0117.0234

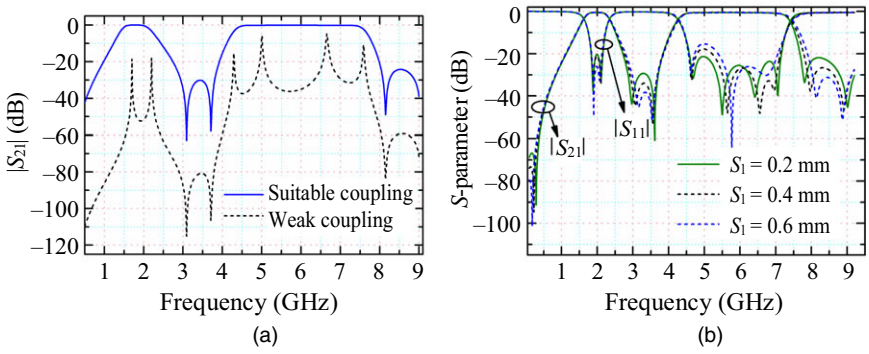

Fig. 4. (a) Frequency response of $|S_{21}|$ operated at ON mode with c = 1.1 pF, and (b) S-parameter versus varied S_1.

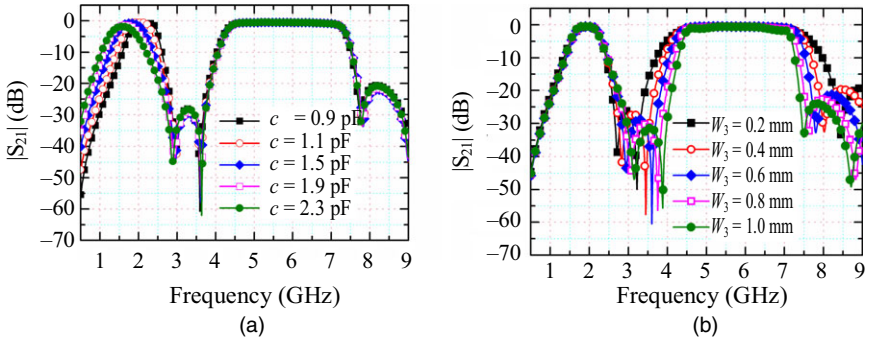

Fig. 5. Frequency response of $|S_{21}|$ operated at ON mode with varied (a) capacitor and (b) W_3.

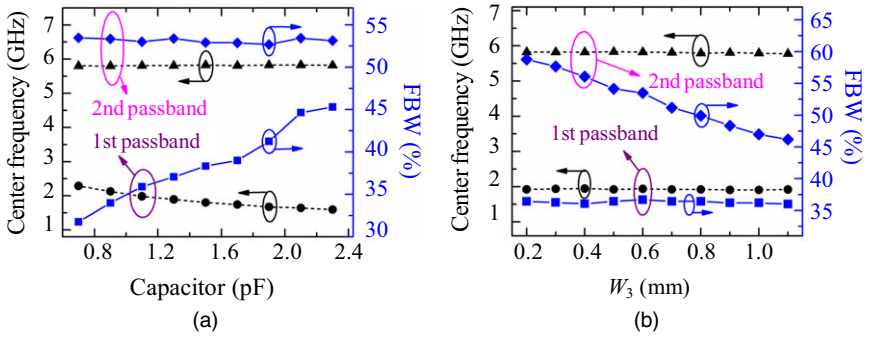

Fig. 6. CFs and FBWs with varied (a) capacitor and (b) W_3.

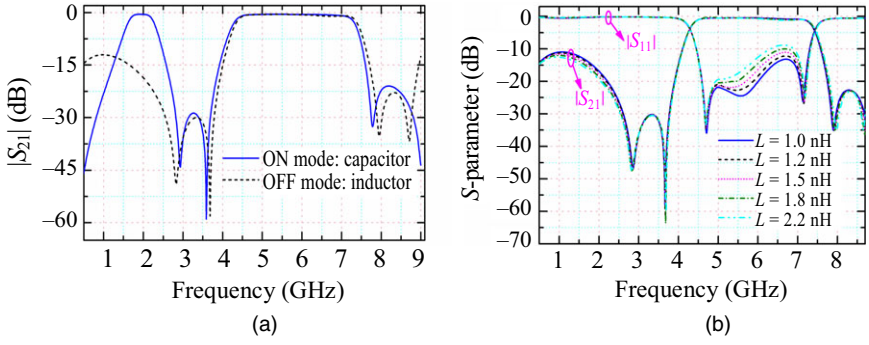

Fig. 7. (a) Comparison of frequency responses of $|S_{21}|$ under ON mode and OFF mode and (b) frequency responses of SWB BPF versus varied inductance L.

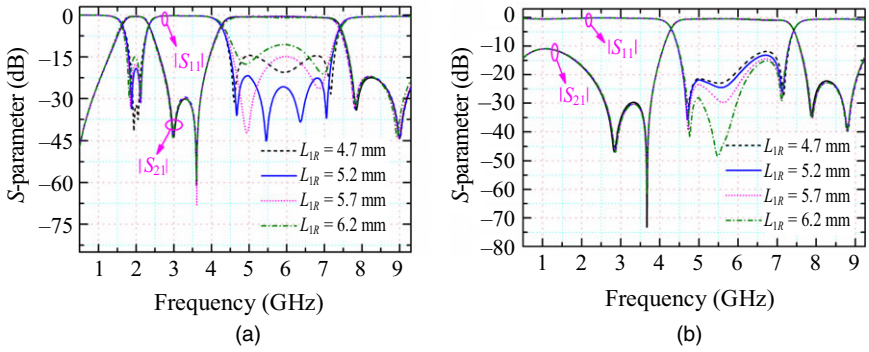

Fig. 8. Frequency responses of (a) DWB BPF and (b) SWB BPF versus varied L_{1R}.

wave electromagnetic simulator with varied inductor values, as shown in Fig. 7(b). It can be observed that the return losses will be better as the inductor's value decreases.

Figure 8(a) and 8(b) show the frequency responses of an SWB-to-DWB BPF with varied L_{1R} under a fixed L_1. Here, the parameter L_{1R} represents the switch position. It can be found that L_{1R} has minor effects on insertion loss, whereas the return loss will be changed as L_{1R} gets large. In order to get the best return loss for an SWB BPF and DWB BPF, L_{1R} = 5.2 mm is chosen.

III. Filter Implementation and Experiment

For verification, a switchable SWB-to-DWB BPF using capacitors and inductors as switch elements is designed and fabricated on a substrate of Rogers 4003C in which ε_r = 3.55, h = 0.508 mm, and tan δ = 0.0027. The specific dimensional parameters of this BPF are listed in Table 1, indicating the overall size is approximately 0.22 $\lambda_g \times 0.068\ \lambda_g$ (excluding the feed lines), where λ_g is the guided wavelength at 1.92 GHz. Figure 9 shows photographs of the fabricated switchable BPFs.

The measured frequency responses are characterized using an Agilent E5071C vector network analyzer (VNA). Figure 10(a) shows the measured $|S_{21}|$ with varied capacitor values on the same tested sample. The minimum insertion losses in passbands with different capacitors are recorded in Fig. 10(b). It can be found that the CF of the 1st passband will shift down from 2.22 GHz to 1.69 GHz when the capacitor values increase from 0.75 pF to 2.2 pF, whereas the 2nd passband is almost unchanged. Correspondingly, its 3-dB passband of the 1st passband can cover the GPS band (1.57 GHz), LTE band (1.8 GHz), and ISM band (2.4 GHz).

Table 1. Dimension parameters of this BPF (uint: mm).

L_{1L}	L_{1R}	L_2	L_3	L_4	L_h	S_1
6.2	5.2	3.05	8.3	8.6	1.2	0.2

W_1	R	W_2	W_3	W_4	W_h	S_2
0.25	0.2	0.3	0.6	0.2	1.4	0.8

The experimental results and simulation results in ON mode (capacitor values are equal to 1.2 pF) and OFF mode (inductor values are equal to 1.2 nH) are shown in Figs. 11(a) and 11(b), respectively. It can be observed from Fig. 11(a) that the measured CFs of a DWB BPF are centered at 1.92 GHz and 5.74 GHz with a 3-dB FBW of

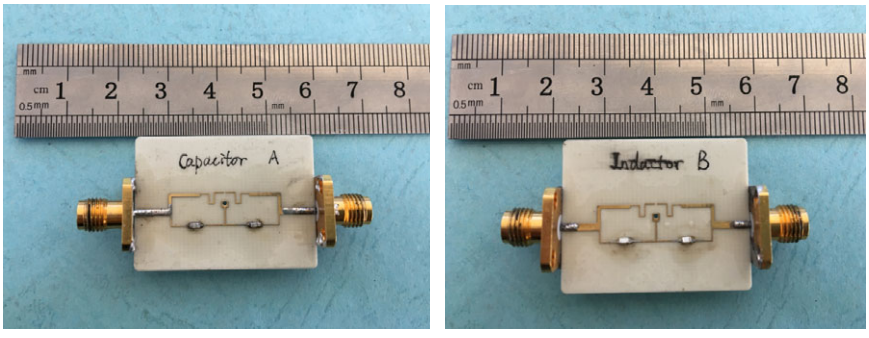

Fig. 9. Photograph of the switchable BPF (a) DWB BPF and (b) SWB BPF.

https://doi.org/10.4218/etrij.17.0117.0234

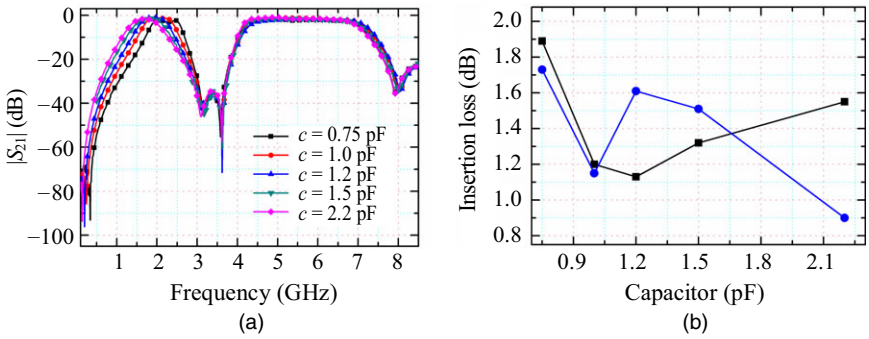

Fig. 10. (a) Frequency response of $|S_{21}|$ and (b) measured insertion loss versus varied capacitor.

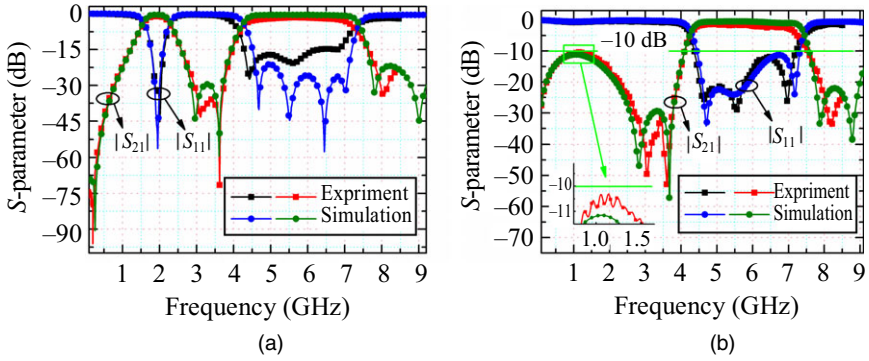

Fig. 11. Comparison between experiment and simulation results under (a) ON mode and (b) OFF mode.

Table 2. Comparison with some reported BPFs.

Filter	CFs (GHz)	3-dB FBWs (%)	Switchable capability	IL (dB)	Size ($\lambda_g \times \lambda_g$)
[1]	3.32/5.32	27.7/19.2	✗	0.62/0.91	0.4 × 0.18
[5]	2.45/5.2	18/4.8	✗	0.6/0.9	0.23 × 0.11
[15]	1.575/1.8/2.4	6.5/3.1/3.5	✗	0.7/0.9/0.9	0.21 × 0.12
[19]	2.34/3.46	25.6/21.4	✗	0.84/1.21	0.21 × 0.2
[25]	1.2/3.5	3.5/4	✓	2.79/2.96	0.21 × 0.064
[26]	1.8/3.5	9/7	✓	–3/–2.3	0.27 × 0.27
This work	1.92/5.74	36.5/49.8	✓	1.13/1.61	0.22 × 0.068

36.5% and 49.8%. The measured insertion loss and return loss of two passbands are 1.13 dB/1.61 dB and 30.9 dB/14.8 dB, respectively. The measured isolation of band-to-band is better than 35.9 dB. Five TZs at 0.26 GHz, 2.97 GHz, 3.61 GHz, 7.82 GHz, and 9.01 GHz are clearly observed from the simulation results. It can be found that the CF of the SWB BPF is centered at 5.75 GHz with a 3-dB FBW of 50.9%. Its measured minimum insertion loss in the passband is 1.4 dB, and the return loss is better than 11.9 dB. Table 2 shows a performance comparison between some reported BPFs and this work in terms of CFs, 3-dB FBWs, switchable capability, insertion loss (IL), and circuit size. The presented BPF shows good performance including wideband, high isolation, compact size, and ability to switch.

IV. Conclusion

In this paper, a switchable SWB-to-DWB BPF, which is switched by alternating the operation mode, is presented. By replacing the lumped switches, reconfigurability is obtained for a same device. The semi-lumped wideband BPF shows good performance including wideband, high isolation, compact size, and ability to switch. This makes the new SWB-to-DWB BPF very attractive with regard to high data rate, high transmission capacity, and multi-functional communication systems.

References

[1] J. Li, S.S. Huang, and J.Z. Zhao, "Compact Dual-wideband Bandpass Filter Using a Novel Penta-Mode Resonator (PMR)," *IEEE Microw. Wireless Compon. Lett.*, vol. 24, no. 10, Oct. 2014, pp. 668–670.

[2] J. Xu, W. Wu, and C. Miao, "Compact Microstrip Dual-/Tri-/Quad-band Bandpass Filter Using Open Stubs Loaded Shorted Stepped-Impedance Resonator," *IEEE Trans. Microw. Theory Tech.*, vol. 61, no. 9, Sept. 2013, pp. 3187–3199.

[3] J. Xu et al., "Compact Single-/Dual-Wideband BPF Using Stubs Loaded SIR (SsLSIR)," *IEEE Microw. Wireless Compon. Lett.*, vol. 23, no. 7, July 2013, pp. 338–340.

[4] J. Li, "Multi-mode Resonators with Quad-/Penta-/Sext-Mode Resonant Characteristics and their Applications to Bandpass Filters," *Int. J. RF Microw. Comput. Aided Eng.*, vol. 27, no. 3, Dec. 2016, pp. 1–12.

[5] H.W. Liu et al., "Compact Dual-Band Bandpass Filter Using Quadruple-Mode Square Ring Loaded Resonator (SRLR)," *IEEE Microw. Wireless Compon. Lett.*, vol. 23, no. 4, Apr. 2013, pp. 181–183.

[6] L. Gao and X.Y. Zhang, "High-Selectivity Dual-Band Bandpass Filter Using a Quad-Mode Resonator With Source-Load Coupling," *IEEE Microw. Wireless Compon. Lett.*, vol. 23, no. 9, Sept. 2013, pp. 474–476.

[7] S.B. Zhang and L. Zhu, "Compact and High-Selectivity Microstrip Bandpass Filters Using Triple-/Quad-Mode Stub-Loaded Resonators," *IEEE Microw. Wireless Compon. Lett.*, vol. 21, no. 10, Oct. 2011, pp. 522–524.

[8] A. Kumar and K.V. Machavaram, "Microstrip Filter with Defected Ground Structure: A Close Perspective," *Int. J. Microw. Wireless Technol.*, vol. 5, no. 5, Aug. 2013, pp. 589–602.

[9] S. Amiri and M. Khajavi, "Improvement the Design of Microwave Dual-Band BPF By DGS Technique," *Microw. Opt. Tech. Lett.*, vol. 58, no. 9, Sept. 2016, pp. 2133–2137.

[10] B. Peng et al., "Wideband Bandpass Filter with High Selectivity Based on Dual-Mode DGS Resonator," *Microw. Opt. Tech. Lett.*, vol. 58, no. 10, Oct. 2016, pp. 2300–2303.

[11] J. Xu et al., "Compact Dual-Band Bandpass Filter Using Single Meander Multimode DGS Resonator," *Electr. Lett.*, vol. 49, no. 17, Aug. 2013, pp. 1083–1084.

[12] J.K. Lee and Y.S. Kim, "Ultra-Wideband Bandpass Filter With Improved Upper Stopband Performance Using Defected Ground Structure," *IEEE Microw. Wireless Compon. Lett.*, vol. 20, no. 6, June 2010, pp. 316–318.

[13] B. Peng et al., "Compact Quad-Mode Bandpass Filter Based on Quad-Mode DGS Resonator," *IEEE Microw. Wireless Compon. Lett.*, vol. 26, no. 4, Apr. 2016, pp. 234–236.

[14] W.J. Feng et al., "High Selectivity Fifth-Order Wideband Bandpass Filters With Multiple Transmission Zeros Based on Transversal Signal-Interaction Concepts," *IEEE Trans. Microw. Theory Tech.*, vol. 61, no. 1, Jan. 2013, pp. 89–97.

[15] H.W. Wu et al., "New Triple-Passband Bandpass Filter Using Multipath Stub Loaded Resonators," *IEEE Microw. Wireless Compon. Lett.*, vol. 26, no. 3, Mar. 2016, pp. 186–188.

[16] C.M. Zhu et al., "Compact QB-BPF Based on Single PMR," *Electr. Lett.*, vol. 52, no. 17, Aug. 2016, pp. 1463–1465.

[17] H.W. Wu et al., "Multi-layered Dual-Band Bandpass Filter Using Stub-Loaded Stepped-Impedance and Uniform-Impedance Resonators," *IEEE Microw. Wireless Compon. Lett.*, vol. 22, no. 3, Mar. 2012, pp. 114–116.

[18] H.W. Liu et al., "Compact Dual-Wideband Bandpass Filter with Multimode Resonator," *ETRI J.*, vol. 36, no. 1, Feb. 2014, pp. 163–166.

[19] J. Li et al., "A Novel Compact Dual-Wideband Bandpass Filter with Multi-Mode Resonators," *Progress Electromagn. Res. Lett.*, vol. 51, no. 6, June 2015, pp. 79–85.

[20] H.W. Liu et al., "Quad-Band Bandpass Filter Using Quad-Mode Stub-loaded Resonators," *ETRI J.*, vol. 36, no. 4, Aug. 2014, pp. 690–693.

[21] Z.H. Chen et al., "Wideband Fully Tunable Bandpass Filter Based on Flexibly Multi-Mode Tuning," *IEEE Microw. Wireless Compon. Lett.*, vol. 26, no. 10, Oct. 2016, pp. 789–791.

[22] J.R. Mao et al., "Tunable Bandpass Filter Design Based on External Quality Factor Tuning and Multiple Mode Resonators for Wideband Applications," *IEEE Trans. Microw. Theory Tech.*, vol. 61, July 2013, pp. 2574–2584.

[23] A. Boutejdar, "Design of 5 GHz-Compact Reconfigurable DGS-Bandpass Filter Using Varactor-Diode Device and Coupling Matrix Technique," *Microw. Opt. Tech. Lett.*, vol. 58, no. 2, Feb. 2016, pp. 304–309.

[24] G.L. Dai and M.Y. Xia, "Design of Compact Dual-Band Switchable Bandpass Filter," *Electr. Lett.*, vol. 45, no. 10, May 2009, pp. 506–507.

[25] S.C. Weng et al., "Compact and Switchable Dual-Band Bandpass Filter with High Selectivity and Wide Stopband," *Electr. Lett.*, vol. 49, no. 20, Sept. 2013, pp. 1275–1277.

[26] B. Lui et al., "Switchable Bandpass Filter with Two-State Frequency Responses," *Electr. Lett.*, vol. 47, no. 1, Jan. 2011, pp. 40–41.

[27] A. Boutejdar, "A New Approach to Design Compact Tunable BPF Starting from Simple LPF Topology Using a Single T-DGS-Resonator and Ceramic Capacitors," *Microw. Opt. Tech. Lett.*, vol. 58, no. 5, May 2016, pp. 1142–1148.

https://doi.org/10.4218/etrij.17.0117.0234

[28] S. Courrèges et al., "A Low Loss X-Band Quasi-Elliptic Ferroelectric Tunable Filter," *IEEE Microw. Wireless Compon. Lett.*, vol. 19, no. 4, Apr. 2009, pp. 203–205.
[29] A. Boutejdar et al., "Design and Optimization of New Compact Tunable 2.4-GHz Band Pass Filter Using Coupled $\lambda/2$ Microstrip Open-Loop Resonators and MEMS-Switch Technique," *Microw. Opt. Tech. Lett.*, vol. 55, no. 10, Oct. 2013, pp. 2444–2450.
[30] Y. Shim et al., "A High-Performance Continuously Tunable MEMS Bandpass Filter at 1 GHz," *IEEE Trans. Microw. Theory Tech.*, vol. 60, no. 8, Aug. 2012, pp. 2439–2447.
[31] A. Boutejdar et al., "Design of Compact Size and Tunable Band Pass Filter for WLAN Applications," *Electr. Lett.*, vol. 52, no. 24, Nov. 2016, pp.1996–1997.

Yang Xiong was born in Huaihua, Hunan province, China, in 1990. He received his BE degree in communication engineering from Shandong University of Technology, Zibo, China, in 2013, and is currently working toward his PhD degree in electronic science and technology at Nankai University, Tianjin, China. His main research interests include microwave circuit design, high-temperature superconducting terahertz devices, and terahertz signal detection.

LiTian Wang was born in Tianjin, China. He received his BE degree in communication engineering from Tianjin University of Science and Technology, China, in 2014, and is currently working toward PhD degree in electronic science and technology at Nankai University, Tianjin, China. His main research interests include microwave passive components and systems, and HTS tunable filter design.

Wei Zhang received his BE degree in communication engineering from Nankai University, Tianjin, China, in 2015, and is currently working toward his ME degree in communication and information system. His main research interests are microwave filters and multiplexer design.

DouDou Pang received her BE degree in communication engineering from Nankai University, Tianjin, China, in 2015, and is currently working toward her ME degree in communication and information system. Her main research interests are microwave filters and antenna design.

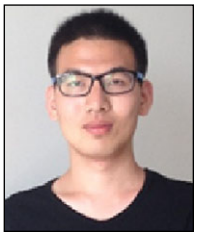

Fan Zhang received his BE degree in communication engineering from Nankai University, Tianjin, China, in 2015, and is currently working toward his ME degree in communication and information system. His main research interests are microwave filters and multiplexers design.

Ming He received his ME and PhD degrees in electrical engineering from Nankai University, Tianjin, China, in 2002 and 2008, respectively. Since 1997, he has been with the Department of Electronics, Nankai University, Tianjin, China, where he became a Professor in 2016. From 2004 to 2009, he held several visiting research appointments in Juelich Research Center and Karlsruhe University, Germany. His research interests are in the fields of the applications of high temperature superconductors, the generation and detection of THz signals, and microwave communications.